Obstacle Induced Branching in Neurospora crassa and Rhizopus oryzae

by

Benjamin Gonzalez

A Thesis Presented in Partial Fulfillment
of the Requirements for the Degree
Master of Science

Approved November 2021 by the
Graduate Supervisory Committee:

Robert W. Roberson, Co-Chair
Debra P. Baluch, Co-Chair
Jeremy Wideman

ARIZONA STATE UNIVERSITY

December 2021

ABSTRACT

The branching dynamics and navigation of filamentous fungi that have an apical vesical crescent (AVC) are poorly understood. Here, *Rhizopus oryzae* (Mucoromycota), which has an AVC, is compared to *Neurospora crassa* (Ascomycota), which has a Spitzenkörper (Spk), as they navigated microfluidic maze environments varying in pattern. The different maze patterns (diamonds, squares, and chevrons) presented increasing angles of impact, and degrees of obstruction. This investigation addressed questions regarding advantages or disadvantages that a Spk or AVC may provide in hyphal growth. All branching phenomena were compared to the regular branching of unobstructed growth to determine obstacle induced branching. *Neurospora crassa* generated more branches per impact amongst all three maze types and was unable to complete the chevron maze types. *Rhizopus oryzae* generated less branches per impact but was able to complete every maze type. The greatest difference in branch formation was seen in the chevron maze design where *N. crassa* generated a greater number than *R. oryzae*. *Neurospora crassa* exhibited a hyperbranching response in the chevron mazes not seen in *R. oryzae*. Closer inspection of the hyperbranching events revealed that they were composed of initial branching events followed by secondary and tertiary branching events. The directional memory of *N. crassa* was also observed, and was a characteristic of *R. oryzae*. While the branching dynamics and navigation of *N. crassa* and *R. oryzae* were different, and *N. crassa* exhibited branching and navigational phenomenon that *R. oryzae* did not, *R. oryzae* seemingly had the advantage with its use of an AVC over *N. crassa*, as it was able to complete every maze type, which *N. crassa* was unable to do.

ACKNOWLEDGMENTS

TABLE OF CONTENTS

LIST OF FIGURES

iv

INTRODUCTION

Investigations into the various navigational mechanisms of fungal hyphae have benefited from new microfabrication technologies used to create microfluidic growth devices (Millet *et al.*, 2019). These devices contain precisely designed growth barriers that allow researchers to visualize hyphal reactions. Recent work using microfluidic mazes has been performed with growing hyphae of the filamentous fungus *Neurospora crassa* (Ascomycota), a model organism in molecular biology. This work highlighted the directional memory of the growing hyphae and visualized branching behaviors (Held *et al.*, 2019). Methods utilizing microfluidic mazes have not been used to investigate filamentous fungi such as *Rhizopus oryzae* (Mucoromycota), which are evolutionarily divergent to *N. crassa* (Spatafora et al., 2016). Fungi such as *R. oryzae* differ in the cellular organization of their apical tips (Fisher and Roberson, 2016; Spatafora *et al.*, 2016). The current work highlights novel navigational characteristics that may be related to these evolutionary differences.

Filamentous fungi are diverse and successful eukaryotic organisms. They occupy many of the world's terrestrial habitats and perform critical roles in decomposition of organic matter and nutrient recycling; additionally, their associations with other organisms, both plants and animals, range between beneficial (*e.g.*, mycorrhizae) to harmful (*e.g.,* pathogenic) (Devi *et al.*, 2020). Fungi are also important in the food and pharmaceutical industries and serve as model organisms in studies of molecular and cellular biology (Bennet, 1998; Palm, 2001). Each environment that fungi inhabit contain diverse microenvironments in which they have evolved. The ability to navigate these microenvironments is crucial to their success. Elucidating the navigation of filamentous

fungi through their microenvironments and the underlying molecular regulatory mechanisms therein have significant benefits to society. For example, such understanding could result in development of novel anti-fungal treatments that inhibit these mechanisms aiding in the prevention of fungal infection and establishment of disease in plants and animals (Lui *et al.*, 2015). Additionally, the navigation and growth of fungal hyphae could provide insights into novel mechanisms of growth and development of other cell types. For example, plant root hairs and pollen tubes, and mammalian neuronal growth share fundamental characteristics that can draw comparison with fungal hyphal extension, such as membrane recycling, cytoskeletal organization, and cytoplasmic flow (Stiess and Bradke, 2011; Schmidt and Haucke, 2007; Mendrinna and Persson, 2015; Riquelme, 2018).

When the polarized growth of fungal hyphae is obstructed, the cells undergo different morphological responses that can result in the reorientation of the growth axis or the formation of new branching hyphae. The branching characteristics of hyphae is often observed as subapical branching, which work in tandem with tropic responses to navigate external stimuli or obstacles (Brand *et al.*, 2007; Brand and Gow, 2009; Riquelme *et al.*, 2018; Held *et al.*, 2019; Harris, 2019). Apical branching (i.e., dichotomous branching) is rare in hyphae but can result from the mechanical obstruction of a growing hypha that results in the immediate formation of new hyphae at the point of impact (Held *et al.* 2019). Sub-apical branching occurs a distance below the tip, either in response to obstacles or as part of control growth morphologies (Harris, 2008; Wolkow *et al.*, 1996). *Rhizopus oryzae* and *N. crassa* were chosen for this comparative study because of their evolutionary divergence in the organization of secretory vesicles at the growing hyphal

apex. *Neurospora crassa* has a tight, well-organized cluster of vesicles at its growing hyphal apex known as a Spitzenkörper (Spk) (*i.e.*, apical body) (Brunswick, 1924; Bartnicki *et al.*, 1995; Roberson and Fuller, 1988). *Rhizopus oryzae*, on the other hand, possesses a loosely organized aggregation of secretory vesicles known as the apical vesicle crescent (AVC) (Fisher and Roberson, 2016). Hyphal tip growth is a highly polarized mode of cell growth that requires a robust secretory system for the delivery of materials (*e.g.*, membrane, proteins, cell wall materials) to sites of cell growth. This secretory mechanism results in the self-assembly of an Spk, found most often in the Basidiomycota and Ascomycota, or an AVC present in most Mucoromycota and Zoopagomycota (Girbardt, 1969; Grove and Bracker, 1970; Lopez-Franco and Bracker, 1996; Roberson *et al.*, 2011; Fisher and Roberson, 2016). The Spk is a dynamic complex of secretory vesicles, cytoskeletal elements, and signaling proteins. The AVC appears less complex, though little is known of its composition other than secretory vesicles. The Spk and AVC act as reception and delivery centers of secretory vesicles during the final stages of secretion resulting in cell extension. These vesicle aggregates are ephemeral, and their presence is positively correlated with optimal rates of hyphal growth (Girbardt, 1957; López-Franco and Bracker, 1996; Fisher and Roberson, 2016; Riquelme *et al.*, 2018). The Spk position and movements within the hyphal apex correlate with the direction of hyphal growth and have recently been implicated in a type of navigational memory in growing hyphae (Girbarbt ,1957; Batnicki-Garcia *et. al.*, 1995; Lopez-Franco and Bracker ,1996; Riquelme *et al.*, 1998; Roberson *et al.*, 2010; Fisher *et al.*, 2018; Held *et al.*, 2019). It is not known if the AVC plays similar navigational roles as the Spk (Fisher *et al.*, 2018).

The molecular mechanisms underlying obstacle-induced branching behaviors in fungal hyphae containing Spk are not well understood. This paucity of knowledge is even greater in fungal hyphae containing an AVC. The objective of this work is to document the differences in hyphal behaviors between hyphae containing Spk (*e.g.*, *N. crassa*) and those containing AVCs (*e.g.*, *R. oryzae*) during growth obstruction. The primary question being addressed is whether the Spk provides advantages to hyphal growth while negotiating their microenvironments.

MATERIALS and METHODS

Organisms and Culture Media

The wild type strain of *Neurospora crassa* (FGSC 988) was obtained from the fungal

Genetics Stock Center (Department of Microbiology, University of Kansas Medical

Center, Kansas City, KS) and the wild type strain of *Rhizopus oryzae* (NRRL 43880)

from the Agricultural Research Service Culture Collection (National Center for

Agricultural Utilization Research, Peoria, IL). *Neurospora crassa* was maintained on

Vogel's complete medium (VCM) (Vogels, 1956) at ~23°C. *Rhizopus oryzae* was

maintained on potato dextrose agar (PDA, Sigma-Aldrich, St. Louis, MO) (Edgerton,

1908) at ~23°C. Liquid cultures of both fungi were grown by inoculating 125ml

Erlenmeyer flasks plugged with sterilized cotton and filled with 50 ml of VCM broth for

N. crassa or potato dextrose broth (PDB) for *R. oryzae*. Both fungal cultures were started

using isolated conidial suspensions. Liquid cultures were grown at ~23°C on an Innova

2150 shaker (New Brunswick Scientific, Edison, NJ) at 125 rpm for 24 hrs before

inoculating the microfluidic chambers.

Experimental Design

Hyphae grown in liquid culture of both *N. crassa* and *R. oryzae* were used as inoculum

for the microfluidic maze chambers. Maze chambers were provided by the NIH

BioMEMS Resource Center (BMRC, BioMEMS Resource Center, Charlestown, MA).

Each maze chamber contained three types of growth obstacles: squares, diamonds, or

chevrons (Fig. 1). The navigation of growth barriers was imaged using live cell imaging with phase contrast light microscopy. Unobstructed hyphal growth of both fungi (Fig. 2) was used as a control. Microfluidic mazes were constructed within a 35 mm Petri dish (Fig. 2d) with barriers that were 10 µm in height. The square mazes presented nearly perpendicular barriers, the diamond mazes presented barriers that would cause the hyphae to impact at acute angles, and the chevron mazes presented barriers that would result in the bending and reorientation of the hypha (Fig. 2a-c). The branching responses were then characterized by the number of resulting branches, the distance from the hyphal tip to the emerging branch, and the branching angle. Values were compared to those of control hyphae growth.

Inoculation of Microfluidic Chambers

Chambers were filled with appropriate broth. Mycelia fragments were placed within the microfluidic chambers through the inoculation port using sterilized fine-tipped forceps. Samples were allowed to recover and grow at room temperature within a humidity chamber. Hyphae grew and typically entered the maze chambers 3 to 5 hrs after placement within the chamber.

Light Microscopy

Upon entry into the maze chambers time-lapse videos were collected using an EVOS-FL Auto Microscope System (Life Technologies, Carlsbad, USA). Videos were recorded using phase contrast optics with a PH2 fluotar 20x objective (NA 0.40) or a PH2 fluotar

40x objective (NA 0.65). Videos were taken over the course of five hours with intervals of 28-60 secs between each image.

Data Analysis

Videos were analyzed using ImageJ-FIJI software (Schindeli et al., 2012). The distance from the apex of the hypha and the first initial branching point was taken for 60 hyphae of *N. crassa* and *R. oryzae* growing unhindered across agar. This was then compared to measurements taken in the same fashion of the branching distances during obstacle-induced branching events. Additionally, the initial impact angles and the number of resulting branches were recorded. Further analysis of eight hyperbranching events in *N. crassa* was carried out by measuring the outer perimeter of the event during the duration of the response. The resulting data sets were statistically analyzed using Microsoft excel (Microsoft Corp., Redmond, WA). Image plates were constructed using Adobe Photoshop 21.0.2 (Adobe Inc., San Jose, CA).

RESULTS

Results of this work were based on the direct comparisons between *N. crassa* and *R. oryzae* hyphal growth characteristics as they navigated through three types of microfluidic maze designs. These growth characteristics included: i) time required to complete growth through mazes ii) hyphal branching dynamics (e.g., subapical branching or hyperbranching), and iii) hyphal behavior during obstacle impact (e.g., directional memory).

i) Maze Completion

Neurospora crassa and *R. oryzae* were compared in navigational behavior and branch formation using microfluidic chambers (Fig. 1). These chambers were 10 µm in height and restricted hyphal growth above and below each obstacle. Three maze patterns filled the chamber presenting growing hyphae with square, diamond and chevron obstacles. Each obstacle design served to present increasing angles of impact to growing hyphae. An initial comparison of *N. crassa* and *R. oryzae* was performed to broadly compare their unique navigational differences as the grew through each maze type. *Neurospora crassa* required longer times to grow through the mazes, except the square mazes, taking approximately 9, 5, and 2 hrs to complete the chevron, diamond, and square mazes, respectively (Figs. 3-5). In the diamond and chevron mazes his was approximately double the amount of time it took *R. oryzae* to complete the mazes (Figs. 3-5). Interestingly, *N. crassa* covered more area within each individual maze (Figs. 3-5) and often circumvented obstacles numerous times (Figs. 3H, 4H, 5H). For example, within diamond mazes *N. crassa* hyphae occupied up to half of the chamber space before exiting the maze (Fig. 4

8

E-H), while a single primary hypha of *R. oryzae* traversed and exited the maze before abundant secondary hyphal branches completed the maze (Fig. 4 A-D). Hyphae of *R. oryzae* did not encircle obstacles (Figs. 3-5). It is notable that *N. crassa* never completely grew through the chevron mazes and 33% of the time only grew to the second row of obstacles, over twelve observations (Fig. 6). During 12 observations of the chevron mazes, *R. oryzae* completed the maze 83% of the time and 16% of the time stopped at the third row of obstacles (Fig. 6).

ii) Branching Dynamics

In order to better understand whether branching was influenced by hyphae impacting growth barriers and not a result of natural branching in filamentous fungi, control branches were measured during unobstructed growth for both fungi grown on appropriate semi-solid growth media (Fig. 2). *Neurospora crassa* was found to branch on average 58.6 µm from the tip during unobstructed growth (STD = 18.6, N = 60), and *R. oryzae* branched on average 56.5 µm from the tip (STD = 16.2, N = 60). Overall characterization of the impact angle and the distance of the emergence of the first branch from the tip revealed a weak negative correlation, with increasing impact angle resulting in a decreasing distance from the tip for the first branch for both *N. crassa* (R^2 = 0.2497) and *R. oryzae* (R^2 = 0.3316) (Fig. 7 A-B). When comparing the number of resulting branches during impacts for each maze type chevron obstacles generated the most branches from impacts, with *N. crassa* averaging 4.7 branches (STD = 2.5, N = 22) and *R. oryzae* averaging 1.0 (STD = 1.3, N = 32) (Fig. 7 C-D). In the square mazes *N. crassa* averaged 0.81 branches (STD = 0.59, N = 21), and *R. oryzae* averaged 0.43 (STD = 0.62, N = 52)

(Fig. 7 C-D). In the diamond mazes *N. crassa* averaged 1.1 branches (STD = 0.44, N = 20), and *R. oryzae* averaged 0.37 (STD = 0.63, N = 68) (Figs. 7 C-D).

When directly comparing the branching dynamics at the tips of the navigating hyphae, similar patterns were seen in the square mazes, but not the diamonds and chevrons. The square mazes presented the growing hyphae with obstacles perpendicular to their axis of growth. *Neurospora crassa* and *R. oryzae* exhibited hyphal branching at or near their tips when impacting the square obstacles at angles near 90 degrees (Figs. 3, 8, 9). *Neurospora crassa* subapically branched upon impacting the square obstacle, as did *R. oryzae* (Figs. 8, 9). For both *N. crassa* and *R. oryzae* the resulting branches would continue growth along the side of the square obstacle opposite to that of the initial impacting hypha (Figs. 8, 9). This pattern would continue down the length of the square maze until the end of the maze was reached for both fungi (Fig. 3). Within the diamond mazes, *N. crassa* exhibited subapical branching, during acute impacts with the diamond edges (Figs. 10). *Rhizopus oryzae* also exhibited subapical branching after impacting an edge of the diamonds (Fig. 11). The major difference in the diamond mazes was the increased area covered by *N. crassa.*

For both *N. crassa* and *R. oryzae*, the chevron mazes presented different branching patterns than the square and diamond mazes (Figs. 12, 13). *Rhizopus oryzae* still exhibited subapical branching within chevron mazes, but generated more branches overall then it did in the square and diamond mazes (Figs. 5, 7, 13). These branching events within the chevrons did not always result in hyphae that traversed the obstacles but ultimately *R. oryzae* was able to complete the mazes and navigate obstacles within the chevrons mazes (Figs. 5 A-D, 6). *Neurospora crassa* experienced a hyperbranching

10

morphology observed within the chevron mazes (Fig. 12). The hyperbranching often

resulted in the individual chevron obstacle not being traversed (Figs. 6, 12). The chevron

mazes were not completed by *N. crassa* over the course of this entire work (Fig. 6). To

the best of our knowledge, hyperbranching behavior has not been previously

documented. Hyperbranching morphology results in the cessation of exploration within

the region of the obstacle and apparent hyphal senescence within the hyperbranching area

(Figs. 5, 6, 12). The hyperbranching events in *N. crassa* were a consistent phenomenon

that became a major focus of this work. Though irregular branching was observed in the

chevron mazes with *R. oryzae* (Fig. 13) these events did not exhibit the same

characteristics as those of the hyperbranching responses of *N. crassa*. When observed at

an increased magnification, the hyperbranching events were revealed to contain several

branching events occurring in a cascade that had a primary hypha developing secondary

branches, which intern generated tertiary branches (Fig. 14). The branching cascades

observed continued to extend into the edge of the chevron obstacle and it is unclear if

quaternary branches continue to form (Figs. 15, 16). The hyperbranching cascade was

also observed to form against the edge of the obstacle, even when one side of the

branching hyphae is exposed to an open area (Figs. 14, 15, 16). The hyper branching

cascade also continued in limited spaces and often resulted in the compaction of the

branching hyphae within the area of the obstacle, at times completely filling the available

space within the beginning of the chevron mazes (Fig. 5, 14). The hyperbranching events

often failed to overcome the obstacles despite the number of branches formed and

resulted in the cessation of growth in all generated hyphae compacted within the

hyperbranching event (Fig. 5). The combination of the compaction within the area, and

the unclear delineation of resultant hyphal branches within the hyperbranching event, present difficulties in characterizing the emergence of branches over time. In order to characterize this the events were manually traced, and the internal area of the trace was taken over time (Fig. 17). The resulting changes in area depicted a consistent pattern that contained and initial burst of branching activity, with a leveling off that occurs around the hour mark of the event (Fig. 18). The decrease in expansion seen at the hour mark correlated with the cessation of growth within the area of the hyperbranching event, and the compaction of the hyphae within the area of the obstacle (Fig. 14) and was often followed by the halt of exploration within the chevron maze over all (Fig. 5).

iii) Directional Memory

The directional memory previously seen in *N. crassa* and described by Held *et al.* in 2019 was also observed here (Fig. 19). Secondary effects of the directional memory in *N. crassa* were increased maze completion times and increased area coverage within the square and diamond mazes, often resulting in the navigating hyphae completely encircling obstacles (Figs. 3, 4, 8, 10). The increased area of coverage was particularly evident in the diamond mazes were *N. crassa* circumvented the diamond obstacles, even when this took the growing hyphae toward the entrance of the maze, this behavior was not observed in *R. oryzae* (Figs. 4, 10). *Rhizopus oryzae* did switch between the edges of the diamond maze channels, switching to the opposite side than that of the previous impact (Fig. 11B-E). This switching of sides was observed many times over the course of this work, but there was no observation of the same directional memory seen in *N. crassa*.

DISCUSSION

The goal of this work was to document hyphal growth behaviors of *N. crassa* and *R. oryzae* as cells negotiated specific growth obstacles that were incorporated into microfluidic chambers. These fungi were selected because of their evolutionary divergence (*N. crassa*, Ascomycota; *R. oryzae*, Mucoromycota) (Spatafora *et al.*, 2016) and the difference in secretory vesicle organization in the hyphal tips (*N. crassa*, Spk; *R. oryzae*, AVC) (Grove and Bracker, 1970; Riquelme *et al.*, 2016; Fisher and Roberson, 2016). The primary question addressed in this work was whether the Spk provided a competitive advantage to hyphal growth through challenging substrate environments. As previously described above, key difference between *N. crassa* and *R. oryzae* is their vesicle organization in the hyphal apex. In *N. crassa*, and other Dikarya, the Spk has been shown to play key roles in exocytosis of secretory vesicles at the hyphal apex and regulation of hyphal growth direction (Girbardt, 1969; Fischer-Parton *et al.*, 2000; Riquelme *et al.*, 2016). Additionally, previous work has described Spk dynamics particularly relevant to the hyperbranching and navigational characteristic of *N. crassa* observed in the current work; specifically, it's directional memory and the Spk dynamics during branching in microfluidic devices (Held *et al.*, 2019). Directional memory is characterized as the retention of the direction of growth, even when the hypha of *N. crassa* is reoriented by an obstacle, followed by the resumption of the direction of growth once past the obstacle (Held *et al.*, 2019). This is achieved by *N. crassa* through the retention of the Spk position relative to the original direction of growth, during impacts

13

with obstacles (Held *et al.*, 2019). It is believed that the AVC has a similar function of exocytosis regulation, but evidence of its regulatory role in hyphal growth direction is elusive (Fisher and Roberson, 2016).

A primary difference observed between *N. crassa* an *R. oryzae* during maze navigation is that *N. crassa* requires more time to completely traverse mazes and, on occasions is not able to completely move through the mazes. Directional memory of *N. crassa* hyphae, previously described in Held *et al.* (2019), can account for these observations. This phenomenon resulted in *N. crassa* hyphae to 'explore' the mazes more completely and repetitively to the point, at times, of cellular senescence. This is in contrast to *R. oryzae* which did not exhibit characteristics of directional memory or retaining apical orientation as observe in hyphae of *N. crassa*. *Rhizopus oryzae* did exhibit subapical branching patterns that varied in terms of the distance of the first branch emergence from the apex, which *N. crassa* also exhibited. However, *R. oryzae* did not exhibit hyperbranching morphology seen in *N. crassa* in the chevron mazes.

As to the underlying molecular mechanism of the unique behaviors seen in *N. crassa* and absent in *R. oryzae,* it is argued here that they are related to thigmotropic, or mechanical signal transduction, through calcium gradients previously described in *Candida albicans* (Brand *et al.*, 2007; Lui *et al.*, 2015) and Uromyces appendiculatus (Hoch *et al.,* 1987).

Thigmotropic responses result in the re-orientation of the growth axis via mechanosensitive signal transduction through transmembrane proteins (Brand *et al.*, 2007). In *C. albicans* the stretch activated calcium channel Mid1, complexed with the voltage gated calcium channel Cch1 and the membrane protein Ecm7, have been

implicated in sensing these mechanical stimuli resulting in the attenuation of the direction of growth (Brand *et al.* 2007; Held *et al.*, 2019; Lange and Peiter, 2020). The mechanical activation of this protein complex results in a localized influx of calcium which results in downstream signaling that ultimately re-orientates the growth axis (Brand *et al.*, 2007). This calcium signaling pathway is not fully understood but is thought to ultimately act on Bud1, which recruits proteins involved in the formation of a new growth axis, and downstream actin cytoskeleton organization through Cdc42 (Park *et al.*, 1997; Brand *et al.*, 2007; Brand and Gow, 2009;). This link between mechanical stimuli and downstream growth axis organization is relevant to the hyperbranching morphology mentioned above in *N. crassa*. It has been shown that apical branching can result from the mechanical obstruction of a growing hypha (Held *et al.*, 2019). In *N. crassa* apical branching has been shown to follow prolonged deformation of the hyphal tip, resulting in the disappearance of the Spk, and the formation of two or more new Spk (Held *et al.*, 2019). Deformation of the hyphal tip is often in response to impacts with obstacles to hyphal growth. These apical branching events are termed obstacle induced branching responses. Obstacle induced branching is characterized by the physical dynamics of the hyphal impact (Held *et al.*, 2019). This disassociation of the Spk during apical branching events must involve the reorganization of the actin cytoskeleton mesh that underlies that Spk structure which could be affected by the calcium dependent thigmotropic signal pathway (Riquelme *et al.*, 2016)

The role of calcium signaling pathways and the Mid1-Cch1 complex in the hyperbranching morphology seen here is also supported by the change in area over time measured in this work, a consistent aspect of the hyperbranching response. Prolonged

sustained impacts with an obstacle, such as those seen in the chevron maze would result in the sustained influx of calcium, which would eventually be returned to basal levels due to the sequestering of ions within organelles and other downstream participants (Lui *et al.*, 2015). This would correspond with the sudden drop off in expansion seen in the area measurements throughout the hyperbranching events. The branches that are generated in the hyperbranching response in *N. crassa* were also all generated on the side of the primary hypha facing the obstacle. This may be related to the Spk dynamics described in other works, but in a repeated manner due to the sustained contact with the obstacle. In order to investigate this, higher resolution fluorescent microscopy would be necessary to visualize the Spk dynamics in all the branches generated during a hyperbranching response. As to the impact the hyperbranching events have on maze navigation, *N. crassa* was not observed completing the chevron mazes through this entire work and when compared to *R. oryzae* often failed to make it past the second row of chevron obstacles. Considering the dramatic use of resources that the hyperbranching events require, and the initial rapid expansion that is undertaken during them, the chevron mazes may not be completed simply because they challenge the growing hyphae of *N. crassa* too much. There are other factors that must be considered in this experimental set up; however, such as local nutrient and oxygen depletion in the mazes which may be exacerbated by the hyperbranching response. Additionally, *N. crassa* had difficulty entering the chevron mazes at all, which may speak further to the impact of nutrient depletion, oxygen depletion, and an over expenditure of resources contributing to it not completing the chevron mazes.

The directional memory seen in previous work (Held *et al.*, 2019), and in this work as well, may also be attributed to the attenuation of the growth axis due to calcium dependent thigmotropic signaling. The microfluidic experiments of previous work, described a system in *N. crassa* which retained the position of the Spk during impact with obstacles (Held *et al.*, 2019). This retention of the position would allow for the impeded hyphae to resume its direction of growth once free, and severe enough impacts within the apex would result in the disassociation of the Spk and the generation of several new Spk which would result in the generation of branches. The retention of the Spk position relative to the previous direction of growth may be reliant on calcium gradients resulting from calcium influx during mechanical stimulation (Brand *et al.*, 2007; Held *et al.*, 2019). This localized calcium influx may be underlying the directional memory seen here through actin cytoskeleton reorganization in a manner that does not result in the disassociation of the Spk but the retention of its position during impacts. This possible mechanism is important to understanding *N. crassa* behaviors because instances of directional memory would account for the hyphae of *N. crassa* regressing through the maze to explore unexplored areas, which *R. oryzae* did not do. Drawing the connection back to hyperbranching responses, the disassociation of the Spk may be prolonged in hyperbranching events and result in the generation of several new Spk, which in turn would also disassociate to generate more subsequent branches, all dependent on localized calcium influxes stimulating the formation of new Spk at new branch sites. The potential downstream target of this calcium dependent thigmotropic pathway may be predetermined by bud site markers within the membrane of the impacting hyphae such as Bud1p, previously mentioned above (Cullen and Sprague, 2002). Eventually this process

would halt after the sequestering of the calcium influx or the depletion of oxygen and nutrients within the area (Brand *et al.*, 2007; Vrabl *et al.*, 2019).

Subapical branching was seen throughout all the maze runs for *R. oryzae*, which differs from apical branching due to its distance from the tip of the hypha. Subapical branching occurs beyond septation in septum forming fungi, which implies differences in the regulatory mechanisms that underlie it (Wolkow *et al.*, 1996, Harris, 2008). Subapical branching form regularly during unobstructed growth of filamentous fungi (Harris, 2008; Riquelme *et al.*, 2018). In *Aspergillus nidulans* these branch formations are preceded by the occurrence of septin rings which are thought to help establish the polarity of new subapical branches (Harris, 2008). While less is understood about the regulation of subapical branch formation than apical branching and tropic responses, subapical branching is thought to be influenced by hyphal extension rates, mechanisms regulating nuclear division, and the quantity of nuclei in the cytoplasm (Wolkow *et al.*, 1996; Harris, 2008). Notably, *R. oryzae* does not form septa, but these regulatory mechanisms may also be at play in *R. oryzae*.

It was found that the impacts with obstacles were stimulating the generation of branches in both fungi. All impacts used in the larger analysis of branching dynamics in *N. crassa* and *R. oryzae* were within limit set by the control branching statistics, and further revealed a weak negative correlation between impact angle and branching distances. The larger analysis also showed that the chevron obstacles stimulated more branching in both fungi; however, in the chevron mazes there were branches of *R. oryzae* that formed after impacts that were outside of the range set by the control. This means that not all of the branches generated by *R. oryzae* are obstacle-induced. The branches of *N. crassa* seen

18

during impacts were within the range set by the control, indicating that they were obstacle-induced.

As mentioned above, the overarching goal of this work was to seek out any advantages inherent in the difference between the two fungi, and it would seem that in general *R. oryzae* had an advantage, which would also imply an advantage to the use of an AVC. *Rhizopus oryzae* also seemingly had an advantage in lacking the hyperbranching and directional memory seen in *N. crassa*. *Rhizopus oryzae* exemplified this advantage in the chevron mazes where it finished the majority of its runs, which *N. crassa* did not do.

There are several avenues of experimentation which would further elaborate on these phenomena and answer if *N. crassa* is at a disadvantage in traversing the chevron mazes because of the Spk. Specifically, ensuring uniform concentrations of oxygen and nutrients within the microfluidic mazes would control for any local depletion that may result in the premature halt of exploration in both fungi. This would speak to a change in the microfluidics designs themselves. Beyond controlling for nutrient depletion and oxygen depletion, experiments investigating the role of calcium dependent thigmotropism in branching behaviors would elucidate the navigation of both fungi. Calcium channel inhibitors would be particularly useful in investigating whether Cch1-Mid1p is at play in the production of branches in both fungi, and its inhibition may affect the hyperbranching morphology (Brand *et al*., 2007). Additionally, higher magnification fluorescence microscopy of the hyperbranching events, specifically focusing on the dynamics of the Spk, would show if the disassociation and reformation of new Spk is also at play in this hyperbranching morphology. Further investigation into the role of calcium signaling

within the branching events of both fungi could be done through the removal or increase of calcium in growth media within the microfluidic mazes using calcium chelators, or specially formulated calcium rich media. Different calcium channel proteins which play a role in the reduction of calcium ion concentrations, such as Vcx1p and Pmc1p, could also serve as targets for knockout strains of *N. crassa*, which would inform as to the role of intracellular calcium ion concentration on the progression of the hyperbranching response as well as directional memory observed in *N. crassa* (Lui *et al*., 2015). Finally, it would be of interest to fluorescently label Bud site marker proteins in *N. crassa* using transgenic expression of GFP in association with them to determine their role in the formation of new branches during impacts, especially given the dissociation and reformation of the Spk during branching in *N. crassa*.

A major hurdle to future work of this kind is the lack of transgenic strains of *R. oryzae* and a lack of information equal to that of *N. crassa* as to the molecular mechanism involved in its navigation and branching. This is a challenge because such a disadvantage prevents deeper investigations into the dynamics of the AVC during branching, as well as the dynamics of intracellular proteins involved in the calcium dependent thigmotropic signal pathway, and the dynamics of cytoskeletal proteins during these events in *R. oryzae*. While not the focus of this particular work, *R. oryzae* was observed performing interesting behaviors which warrant investigation. Often when impacting within the mazes *R. oryzae* was observed turning starkly toward the wall of the maze channels. This turning was often away from the side of the channel that it previously impacted, which may speak to some type of sensation of its environment that is as of yet undescribed.

Without similar resources to those available in *N. crassa* investigation of these and similar behaviors in *R. oryzae* is severally limited. Without the use of genetic models and fluorescent strains to further investigate the molecular biology of the behavior, work is limited to statistical behavioral analysis without further evaluation of causes. The development of these type of transgenic models and wealth of information is of importance, as *R. oryzae* and other fungi of the Mucoromycota are important as agricultural plant pathogens, and fungal pathogens in humans which cause mucoromycosis (Reid *et al.*, 2020; Anderson *et al.*, 2004).

REFERENCES

Anderson, P.K., A.A. Cunningham, N.G. Patel, F.J. Morales, P.R. Epstein, and P. Daszak. 2004. Emerging infectious diseases of plants: pathogen pollution, climate change and agrotechnology drivers. Trends in Ecology & Evolution. 19:535–544.

Bartnicki-Garcia, S., D.D. Bartnicki, G. Gierz, R. Lopez-Franco, and C.E. Bracker. 1995. Evidence that Spitzenkörper behavior determines the shape of a fungal hyphae: a test of the hyphoid mode. Experimental Mycology. 19:153–159.

Bennett, J.W. 1998. Mycotechnology: The role of fungi in biotechnology based on a lecture held at the symposium, `progress in US biotechnology', at the 8th European Congress on Biotechnology (ECB8) in Budapest, Hungary, August 1997. Journal of Biotechnology. 66:101–107.

Brand, A., and N.A. Gow. 2009. Mechanisms of hypha orientation of fungi. Current Opinion in Microbiology. 12:350-357.

Brand, A., S. Shanks, V.M. Duncan, M. Yang, K. Mackenzie, and N.A. Gow. 2007. Hyphal Orientation of *Candida albicans* Is Regulated by a Calcium-Dependent Mechanism. Current Biology. 17:347–352.

Brunswick, H. 1924. Untersuchungen über Geschlechts- und Kernverhältnisse bei der Hymenomyzetengattung Coprinus. In: Goebel K (ed) Botanische Abhandlung. Gustav Fischer, Jena. Germany.

Cullen, P.J., and G.F. Sprague. 2002. The roles of bud-site-selection proteins during haploid invasive growth in yeast. Molecular Biology of the Cell. 13:2990–3004.
Devi, R., T. Kaur, D. Kour, K.L. Rana, A. Yadav, and A.N. Yadav. 2020. Beneficial fungal communities from different habitats and their roles in plant growth promotion and Soil Health. Microbial Biosystems. 5:21–47.

Fischer-Parton, S., R.M. Parton, P.C. Hickey, J. Dijksterhuis, H.A. Atkinson, and N.D. Read. 2000. Confocal microscopy of FM 4-64 as a tool for analyzing endocytosis and vesicle trafficking in living fungal hyphae. Journal of Microscopy. 198:246-259.
Fisher, K.E., and R.W. Roberson. 2016. Hyphal tip cytoplasmic organization in four zygomycetous fungi. Mycologia. 108:533–542.

Fisher, K.E., I. Romberger, D. Lowry, P. Shange, and R.W. Roberson. 2018. Hyphal tip growth and cytoplasmic characters of *Conidiobolus Coronatus* (Zoopagomycota, Entomophthoromycotina). Mycologia. 110:31–38.

Girbardt, M. 1969. Die Ultrastruktur der Apikalregion von Pilzhyphen. Protoplasma 67:413–441.

Girbardt, M. 1957. Der Spitzenkörper von Polystictus versicolor (L.). Planta. 50:47–59.
Grove, S.N., and C.E. Bracker. 1970. Protoplasmic organization of hyphal tips among fungi: vesicles and Spitzenkörper. Journal of Bacteriology. 104:989–1009.

Harris, S.D. 2019. Hyphal branching in filamentous fungi. Developmental Biology. 451: 35-39.

Harris, S.D. 2008. Branching of fungal hyphae: Regulation, mechanisms and comparison with other branching systems. Mycologia. 100:823–832.

Held, M., O. Kašpar, C. Edwards, and D.V. Nicolau. 2019. Intracellular mechanisms of fungal space searching in microenvironments. Proceedings of the National Academy of Sciences. 116:13543–13552.

Hoch, H.C., R.C. Staples, B. Whitehead, J.Comeau, and E.D. Wolf. 1987. Signalling for growth orientation and cell differentiation by surface topography in Uromyces. Science. 235:1659-1662.

Lange, M., and E. Peiter. 2020. Calcium Transport Proteins in Fungi: The Phylogenetic Diversity of Their Relevance for Growth, Virulence, and Stress Resistance. Frontiers in Microbiology. 10:1-14

Li, X., Y. Hou, L. Yue, S. Liu, J. Du, and S. Sun. 2015. Potential targets for antifungal drug discovery based on growth and virulence in *Candida albicans*. Antimicrobial Agents and Chemotherapy. 59:5885–5891.

Lopez-Franco, R., and C.E. Bracker. 1996. Diversity and dynamics of the Spitzenkörper in growing hyphal tips of higher fungi. Protoplasma. 195:90–111.
Mendrinna, A., and S. Persson. 2015. Root hair growth: it's a one-way street. F1000Prime Reports. 7:1-6

Millet, L.J., J. Aufrecht, J. Labbé, J. Uehling, R. Vilgalys, M.L. Estes, C.M. Guennoc, A. Deveau, S. Olsson, G. Bonito, M.J. Doktycz, and S.T. Retterer. 2019. Increasing access

to microfluidics for studying fungi and other branched biological structures. Fungal Biology and Biotechnology. 6:1-14

Palm, M.E. 2001. Systematics and the impact of invasive fungi on agriculture in the United States. BioScience. 51:141-147.

Park, H.O., E. Bi, J.R. Pringle, and I. Herskowitz. 1997. Two active states of the Ras-related Bud1/Rsr1 protein bind to different effectors to determine yeast cell polarity. Proceedings of the National Academy of Sciences. 94:4463–4468.

Reid, G., J.P. Lynch, M.C. Fishbein, and N.M. Clark. 2020. Mucormycosis. Seminars in Respiratory and Critical Care Medicine. 41:099–114.

Regaladot, C.M. 1998. Roles of calcium gradients in hyphal tip growth: A mathematical model. Microbiology. 144:2771–2782.

Riquelme, M., R.W. Roberson, and E. Sánchez-Leon. 2016. Hyphal tip growth in filamentous fungi. In: Wendland J (ed) Growth, Differentiation and Sexuality, 3rd Edition The Mycota I. Springer International Publishing. Switzerland. pp 47-66.

Riquelme, M., J. Aguirre, S. Bartnicki-García, G.H. Braus, M. Feldbrügge, U. Fleig, and R. Fischer. 2018. Fungal Morphogenesis, from the Polarized Growth of Hyphae to Complex Reproduction and Infection Structures. Microbiology and Molecular Biology Reviews. 82:1-47

Roberson, R.W. and M.S. Fuller. 1988. Ultrastructural aspects of the hyphal tip of *Sclerotium rolfsii* preserved by freeze substitution. Protoplasma. 146:143–149.

Roberson, R.W., E. Saucedo, D. Maclean, J. Propster, B. Unger, T.A. Oneil, K. Parvanehgohar, C. Cavanaugh, and D. Lowry. 2011. The hyphal tip structure of *Basidiobolus sp*.: A zygomycete fungus of uncertain phylogeny. Fungal Biology. 115:485–492.

Schindelin, J., I. Arganda-Carreras, E. Frise, V. Kaynig, M. Longair, T. Pietzsch, S. Preibisch, C. Rueden, S. Saalfeld, B. Schmid, J.Y. Tinevez, D.J. White, V. Hartenstein, K. Eliceiri, P. Tomancak, and A. Cardona. 2012. Fiji: an open-source platform for biological-image analysis. Nature Methods. 9: 676–682.

Schmidt, M.R., and V. Haucke. 2007. Recycling endosomes in neuronal membrane traffic. Biology of the Cell. 99:333–342.

Spatafora, J.W., Y. Chang, G. Benny, K. Lazarus, M.E. Smith, M.L. Berbee, G. Bonito, N. Corradi, I. Grigoriev, A. Gryganskyi, T.Y. James, K. O'Donnell, R.W. Roberson, T.N. Taylor, J. Uehling, R. Vilgalys, and M.M. White. 2016. A phylum-level phylogenetic classification of zygomycete fungi based on genome-scale data. Mycologia 108:1028–1046.

Stiess, M., and F. Bradke. 2011. Neuronal polarization: The cytoskeleton leads the way. Developmental Neurobiology. 71:430–444.

Virag, A., and S.D. Harris. 2006. The Spitzenkörper: a molecular perspective. Mycological Research. 110:4–13.

Vogel, H.J. 1956. A Convenient Growth Medium for *Neurospora crassa*. Microbial Genetics Bulletin. 13: 42-47

Vrabl, P., C.W. Schinagl, D.J. Artmann, B. Heiss, and W. Burgstaller. 2019. Fungal growth in batch culture – what we could benefit if we start looking closer. Frontiers in Microbiology. 10:1-11

Wolkow, T.D., S.D. Harris, and J.E. Hamer. 1996. Cytokinesis in aspergillus nidulans is controlled by cell size, nuclear positioning and mitosis. Journal of Cell Science. 109:2179–2188.

APPENDIX A

OBSTACLE INDUCED BRANCHING IN *NEUROSPORA CRASSA* AND *RHIZOPUS*

ORYZAE
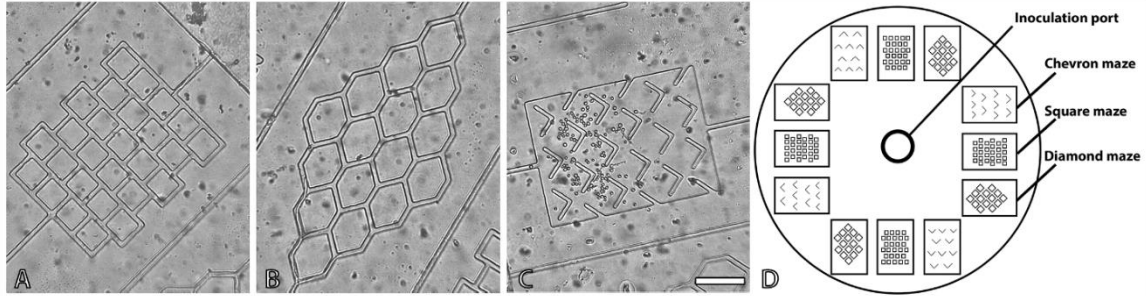
Figure 1. Microfluidic maze design. The microfluidic devices were constructed to have three maze patterns that repeat around the central inoculation port. The different patterns presented varying impact angles and levels of obstruction. (A) The squares introduced perpendicular impact angles. (B) The Diamonds introduced acute impact angles. (C) The chevrons introduced obstacles that were more obstructive. (D) The layout of the microfluidic maze device. The height of maze chambers was 10 µm. Scale bar = 120 µm.
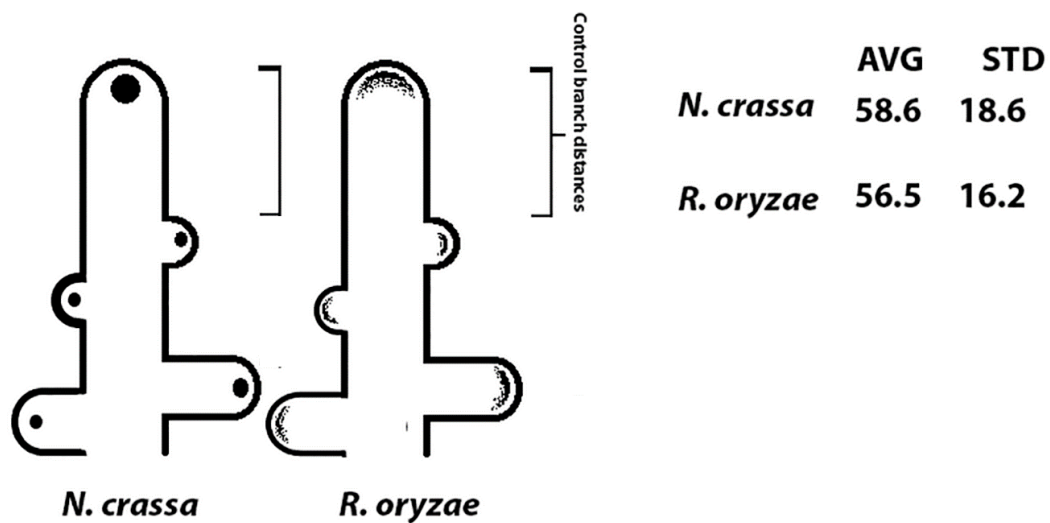
Figure 2. Unobstructed branching distances. Measurements were taken from the hyphal tip to the first emergence of a new branch as an unobstructed growth control. The average control branching distance was 58.4 µm (n = 60; std 18.6 µm) in *N. crassa,* and 56.6 µm (n = 60; std = 16.2 µm) in *R. oryzae.*
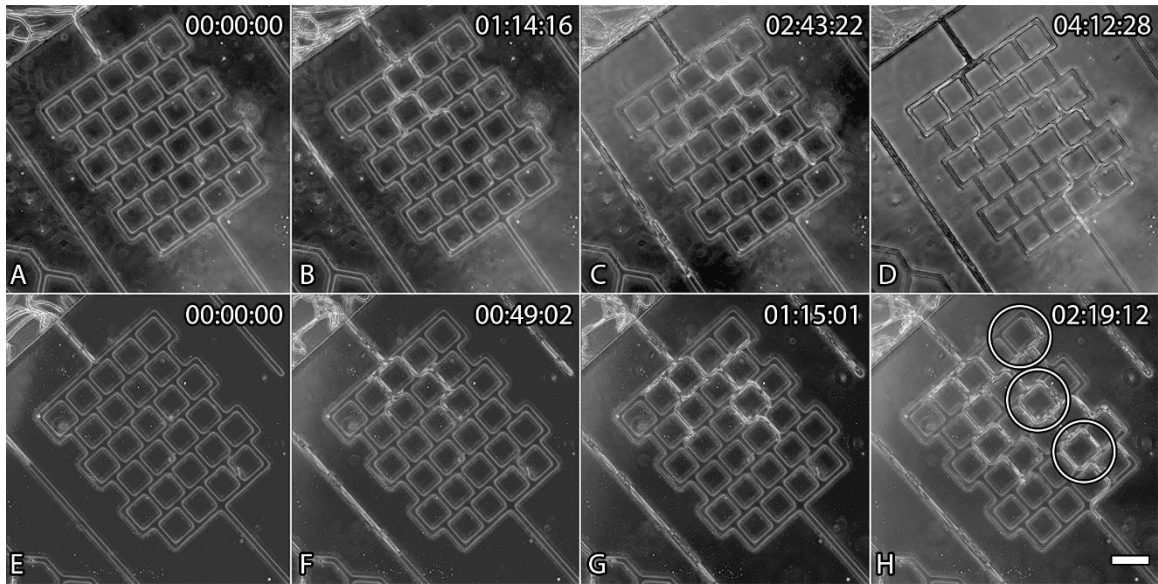
Figure 3. Comparison of *N. crassa* and *R. oryzae* in the square mazes. (A-D) *Rhizopus oryzae* traverses the square maze in 4 hrs and 12 mins with multiple subapical branching events occurring. (E-H) *Neurospora crassa* traverses the squares maze in 2 hrs and 19 mins with multiple subapical branching events occurring. (H) The circles highlight areas were *N. crassa* circumvents squares multiple times. Time stamp = hrs:mins:secs. Scale bar = 40 µm.
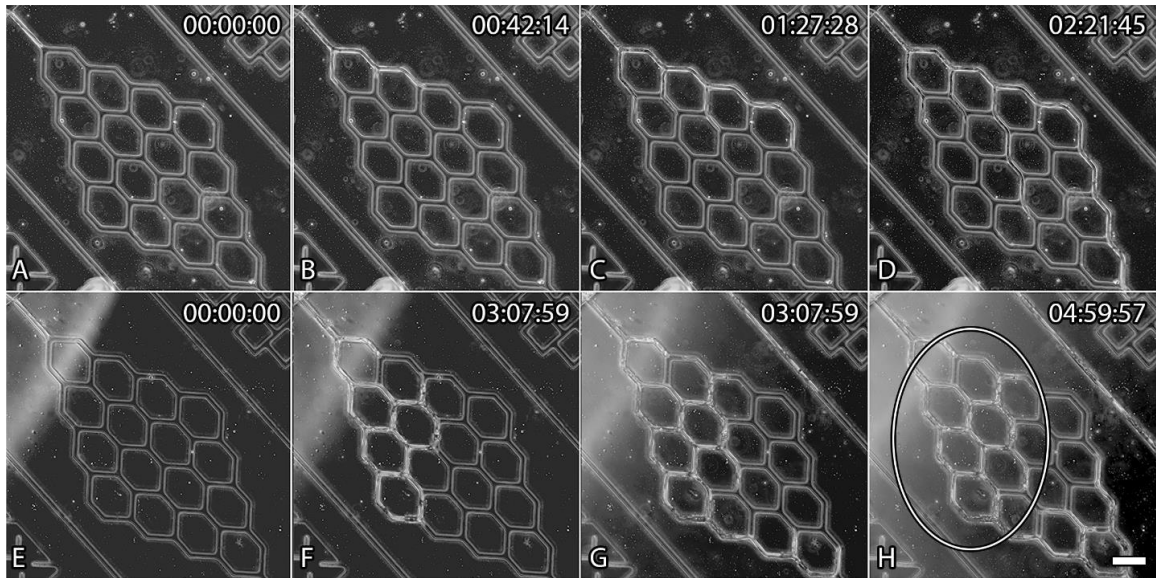
Figure 4. Comparison of *N. crassa* and *R. oryzae* in the diamond mazes. (A-D) *Rhizopus oryzae* navigates the diamond mazes in 2 hours and 21 minutes, and branches subapically throughout. A hypha of *R. oryzae* traverses the maze before abundant branches completed. (E-H) *Neurospora crassa* navigates the diamond maze in 4 hours and 59 minutes, and branches subapically. (H) The circle highlights the areas within the maze were *N. crassa* completely encircled obstacles. Time stamp = hrs:mins:secs. Scale bar = 40 µm.
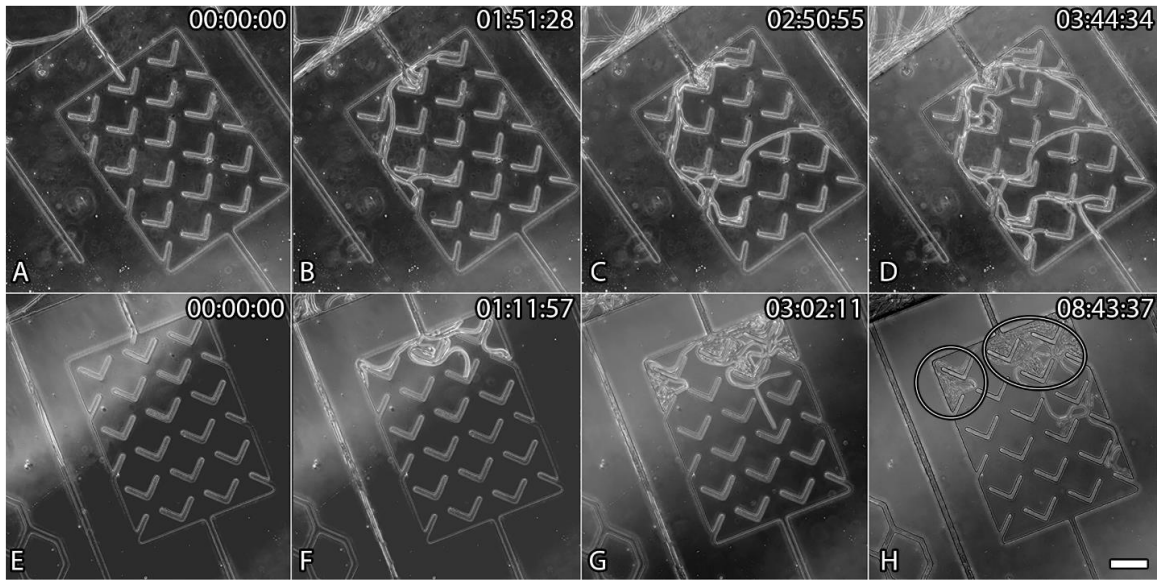
Figure 5. Comparison of *N. crassa* and *R. oryzae* in the chevron mazes. (A-D) *Neurospora crassa* completes the chevron maze in 3 hours and 44 minutes and exhibits an irregular branching pattern. (E-H) *Neurospora crassa* completes the chevron maze in 8 hours and 43 minutes, exhibiting a hyperbranching morphology near the entrance. (H) Circles point out areas of both hyperbranching and circumventing of chevron obstacles. Time stamp = hrs:mins:secs. Scale bar = 40 µm.
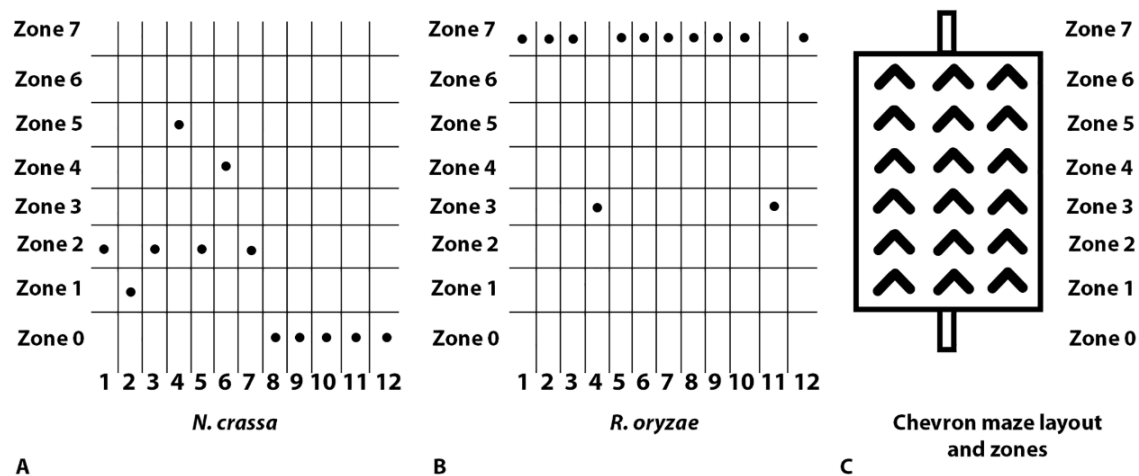
Figure 6. Comparison of *N. crassa* and *R. oryzae* chevron maze completion. (A) *Neurospora crassa* completed the chevron mazes 0% of the time, failed to enter the maze 41% of the time, and made it to the second set of obstacles 33% of the time. (B) *Rhizopus oryzae* completed the maze 83% of the time and stopped at the third row of obstacles 16% of the time. (C) The layout of the chevron mazes broken down into zones, with zone zero representing the entrance and zone seven representing the exit.
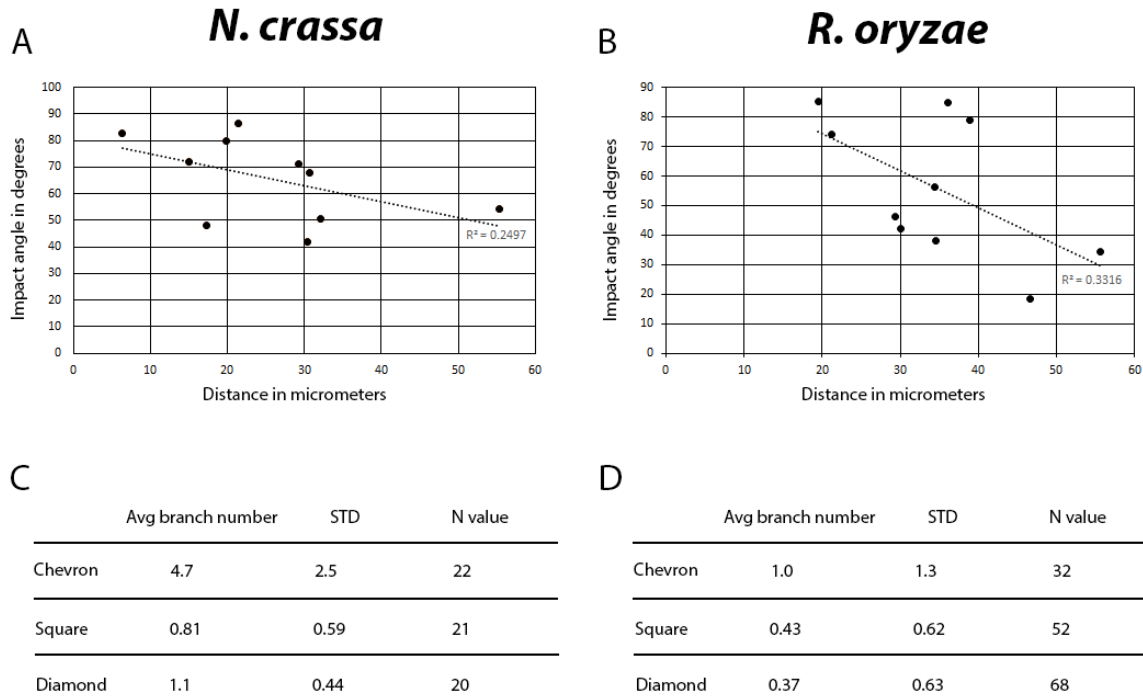
A — N. crassa

(Scatter plot: Impact angle in degrees vs Distance in micrometers; $R^2 = 0.2497$)

B — R. oryzae

(Scatter plot: Impact angle in degrees vs Distance in micrometers; $R^2 = 0.3316$)

C

	Avg branch number	STD	N value
Chevron	4.7	2.5	22
Square	0.81	0.59	21
Diamond	1.1	0.44	20

D

	Avg branch number	STD	N value
Chevron	1.0	1.3	32
Square	0.43	0.62	52
Diamond	0.37	0.63	68

Figure 7. *Neurospora crassa* and *R. oryzae* impact analysis. (A) The distance of the first branch during impacts in micrometers is plotted against the impact angle in degrees for *N. crassa*. There is a negative correlation between impact angle and branching distance ($R^2 = 0.2497$, N = 10). (B) The distance of the first branch during impacts in micrometers is plotted against impact angle in degrees for *R. oryzae*. There is also a negative correlation between impact angle and branching distance for *R. oryzae* ($R^2 = 03316$, N = 10). (C) The average number of branches generated per impact was calculated for each maze type in *N. crassa*. The chevrons averaged 4.7 branches per impact (STD = 2.5, N = 22), the squares averaged 0.81 branches per impact (STD = 0.59, N = 21), the diamonds averaged 1.1 branches (STD = 0.44, N = 20). (D) The average number of branches per impact were calculated for *R. oryzae* in each maze type. The chevrons averaged 1.0 branches (STD =1.3, N = 32), the squares averaged 0.43 (STD = 0.62, N = 52), the diamonds averaged 0.37 (STD = 0.63, N = 68).
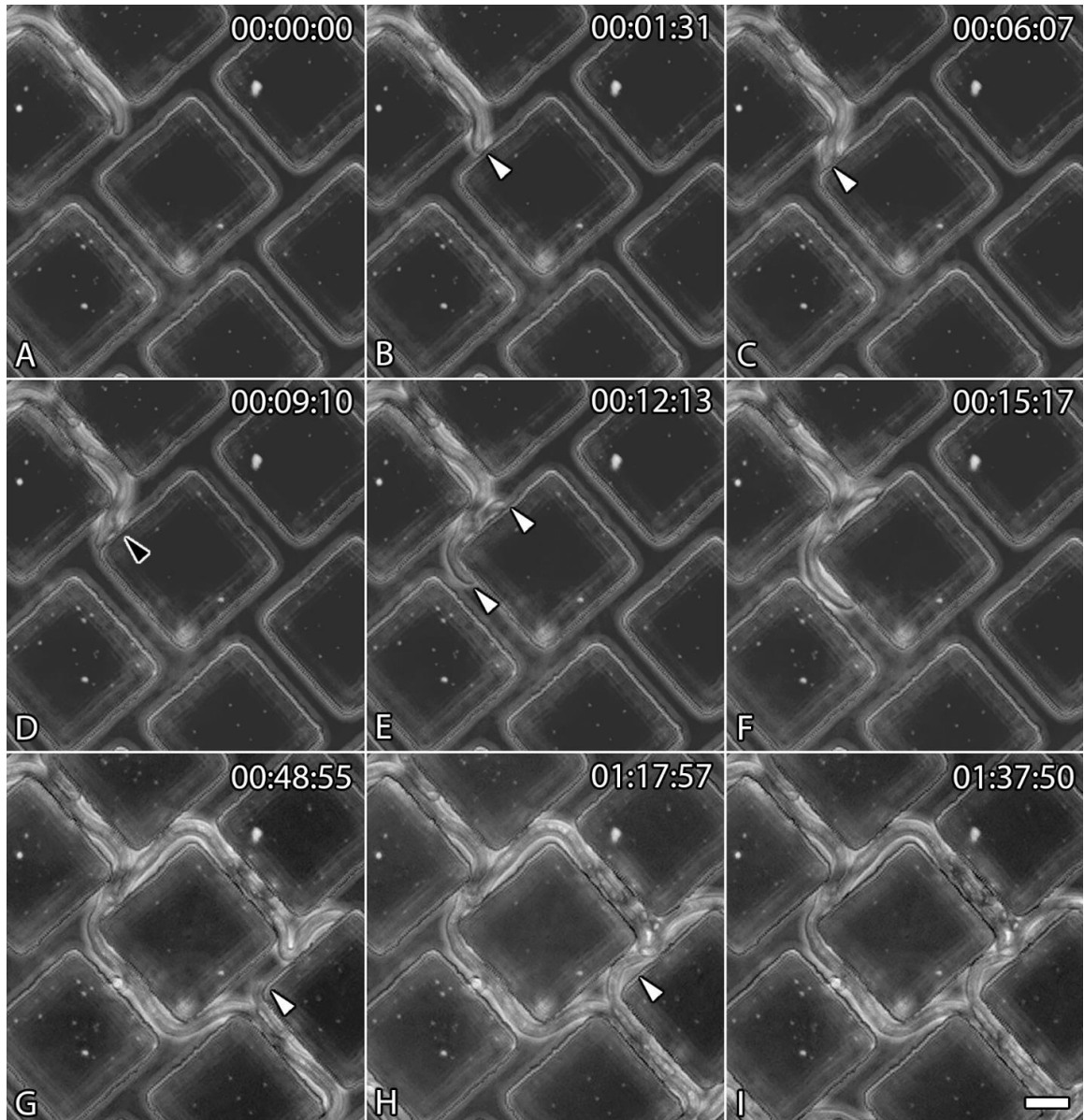
Figure 8. *Neurospora crassa* impacting square obstacles. (A) *Neurospora crassa* enters the chevron maze. (B-C) *Neurospora crassa* impacts the square obstacle then deforms at the tip, with the white arrowhead indicating the point of impact (D) A branch emerges sub apically, the black arrowhead indicates the point of emergence. (E-F) The two hyphae continue extending to either side of the obstacle, with the white arrowheads indicating the two hyphae. (G-I) A hypha is seen regressing through the maze and completely encircling the square, with the white arrowheads indicating the hypha. Time stamp = hrs:mins:secs. Scale bar = 20 µm.
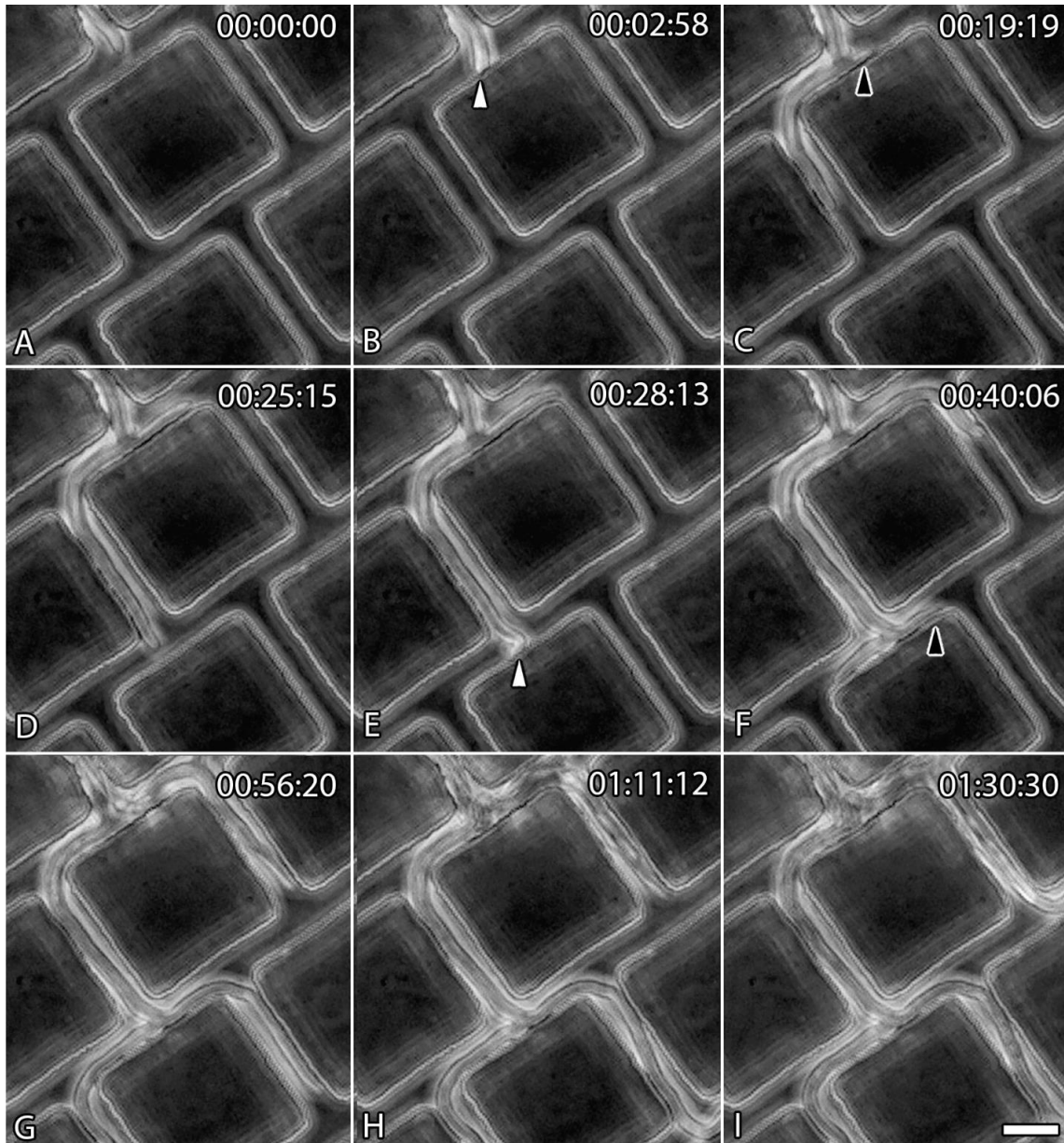
Figure 9. *Rhizopus oryzae* impacting square obstacles. (A, B) *Rhizopus oryzae* enters the mazes and impacts the square obstacle, with the white arrowhead indicating the point of impact. (C) The black arrowhead indicates where a branch emerges sub apically. (D-E) The two hyphae continue to extend to either side of the point of impact before the left hyphae impacts the next square with the white arrowhead indicating the point of impact. (F) The black arrowhead indicates the emergence of a second sub apical branch. (G-H) The hyphae continue to navigate the square mazes in the manner with no instance of regression. Time stamp = hrs:mins:secs. Scale bar = 20 µm.
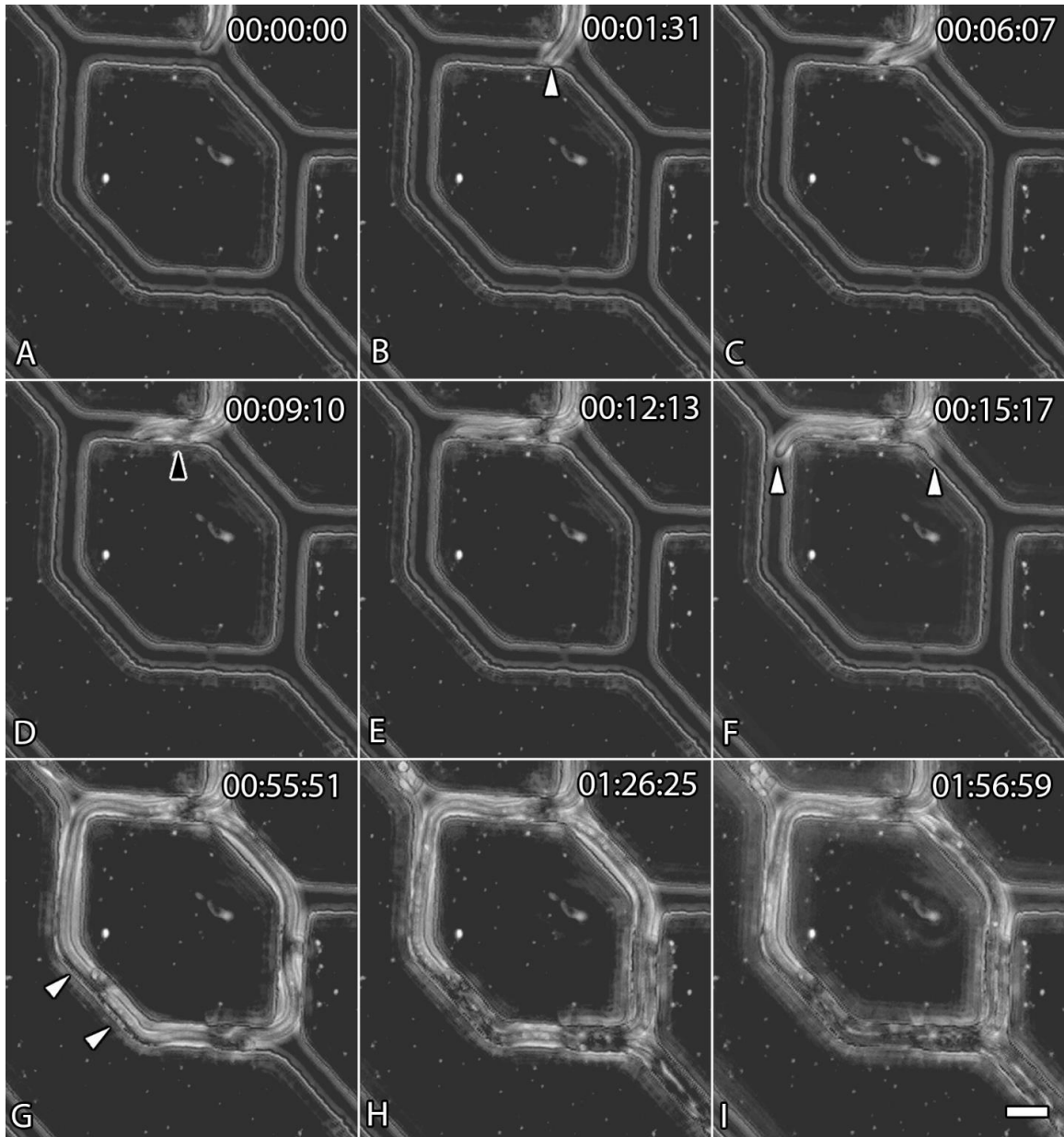
Figure 10. *Neurospora crassa* impacting diamond obstacles. (A-D) *Neurospora crassa* forms a branch impacting the diamond obstacle at a near perpendicular angle forming a subapical branch with (C) The deformation of the tip exhibited. The white arrowhead indicates the point of impact, and the black arrowhead indicates the emerging branch. (D-F) Both branches continue extension laterally to either side of the diamond, before (G-H) completely encircling the diamond obstacle and continuing maze exploration above and below the obstacle. (G) The white arrowheads indicate were the two hyphae meet on the other side of the diamond obstacle. Time stamp = hrs:mins:secs. Scale bar = 20 µm.
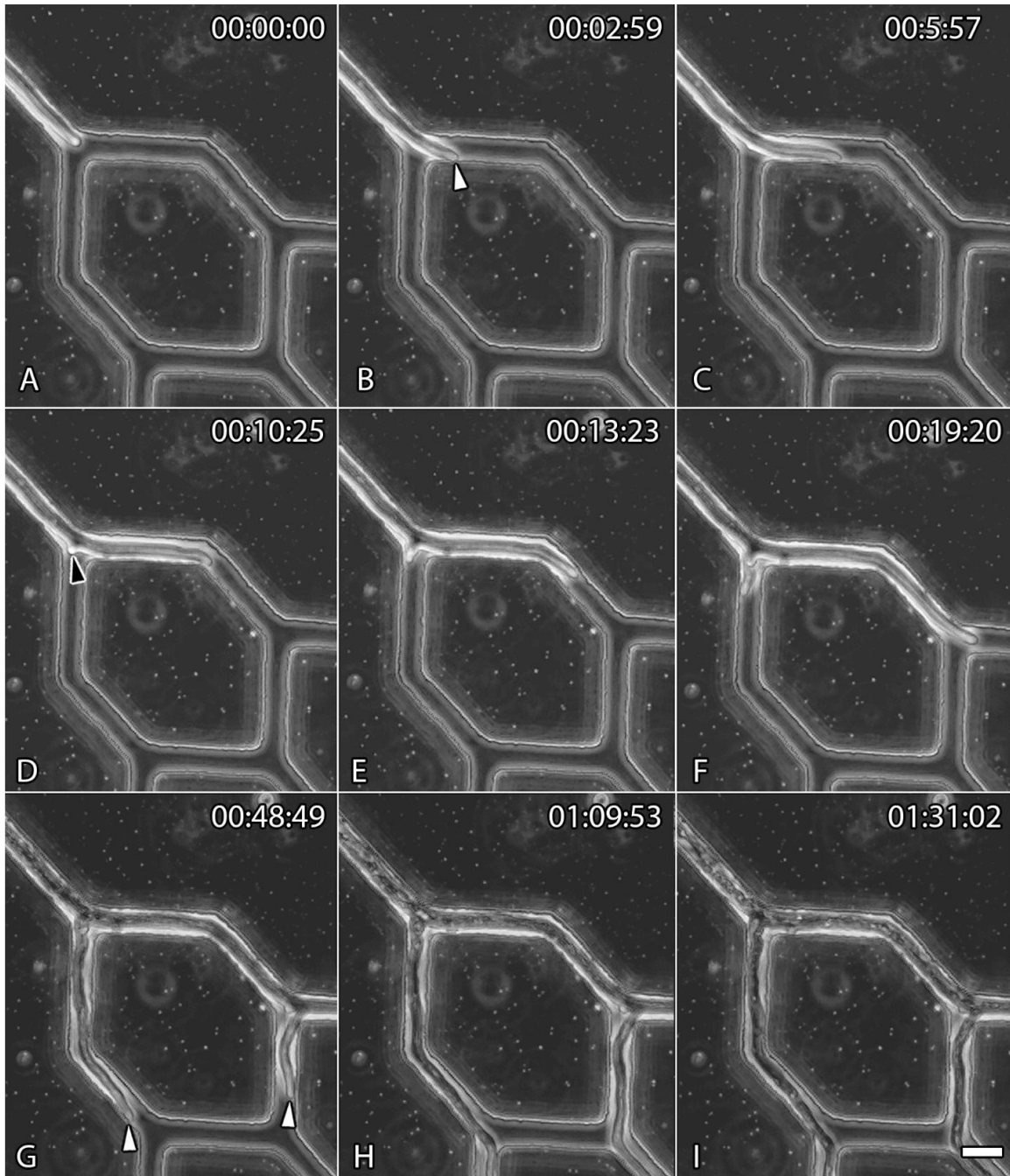
Figure 11. *Rhizopus oryzae* impacting diamond obstacles. (A-C) *Rhizopus oryzae* impacts the diamond obstacles at an acute angle and continues to extend through the right channel. The white arrowhead indicates the point of impact. (D*) Rhizopus* oryzae branches subapically, with the black arrowhead indicating the new branch. (E-I) The subapical branch extends through the opposite channel with another sub apical branch forming at the bottom edge of the diamond obstacle. (G) The white arrowheads indicate the two new subapical branches. Time stamp = hrs:mins:secs. Scale bar = 20 μm.
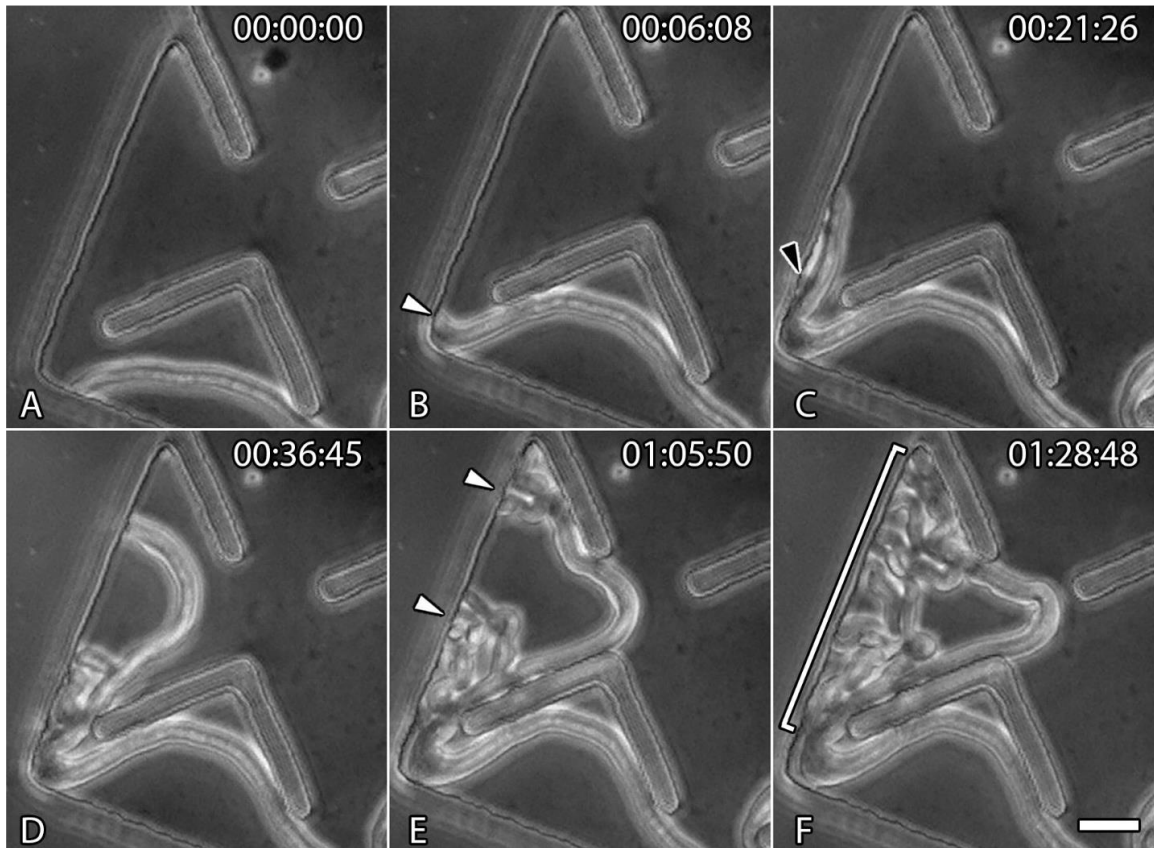
Figure 12. *Neurospora crassa* hyper branches in the chevron maze. (A-B) A hypha of *N. crassa* impacts the corner of the chevron maze and is bent back to a right angle. The white arrowhead indicates the point of impact. (C) The black arrowhead highlights the first emergence of a branch. (D-F) The hypha begins to hyperbranched at two points. (E) the white arrowheads indicate the two points were hyperbranching occurred. (F) The bracket highlights the extent of emerging branches. Time stamp = hrs:mins:secs. Scale bar = 20 μm.
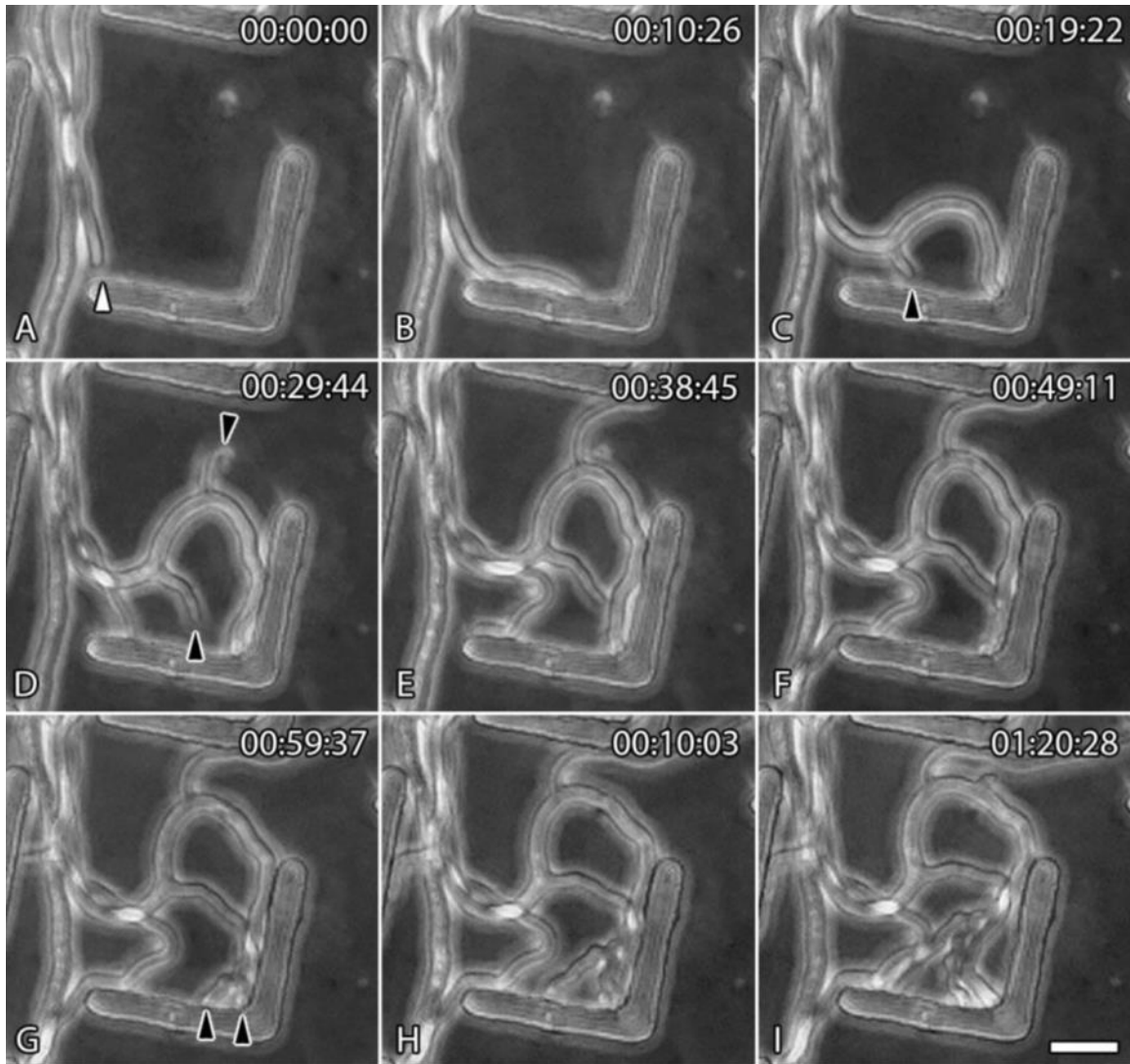
Figure 13. *Rhizopus oryzae* impacting in the chevron maze. (A) *Rhizopus oryzae* impacts the chevron edge, with the white arrowhead indicating the point of impact. (B-C) The hypha travels along the chevron edge before branching subapically, with the black arrowhead indicating the emerging branch. (D) A second subapical branch emerges, with the second black arrowhead indicating the emerging branch. (E-I) The primary hypha continues to push against the chevron edge before branching subapically near the tip. (G) The black arrowheads indicate the two branches near the tip. Time stamp = hrs:mins:secs. Scale bar = 20 μm.
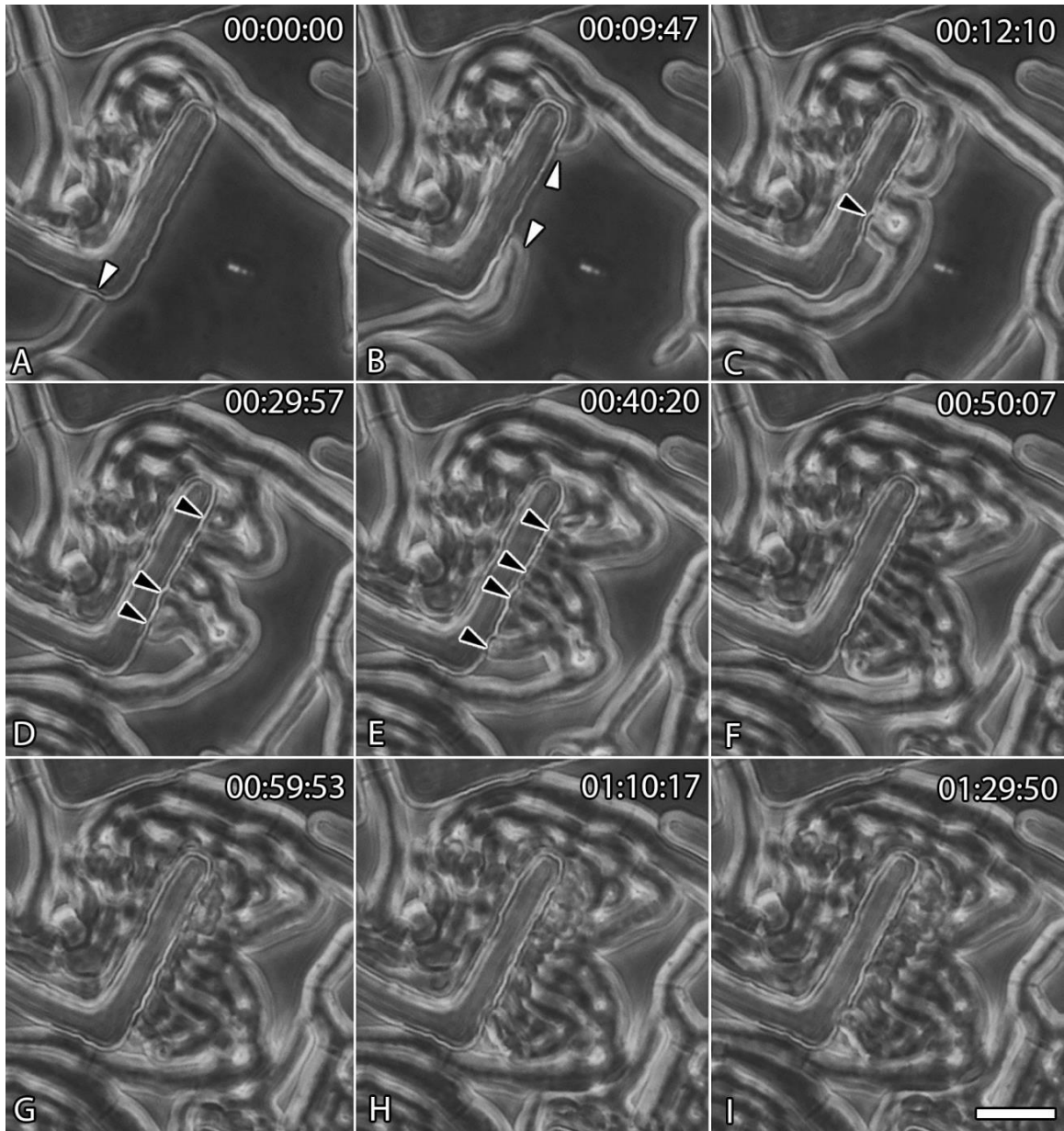
Figure 14. Two hyphae of *N. crassa* hyperbranching. (A) A hyphae of *N. crassa* impacts the chevron on its left side, with the white arrowhead indicating the point of impact. (B) The hyphae of *N. crassa* continues along the chevron edge, while a second hypha round the chevron and travels along the same edge, with the white arrowheads indicating the two hyphae. (C) The hyphae meet in the middle edge and begin to generate branches. (D-F) Secondary and tertiary branches form on both hyphae. (G-I) The hyphae continue to extend, pressing into the chevron edge. The black arrowheads indicate emerging branches. Time stamp = hrs:mins:secs. Scale bar = 40 µm.
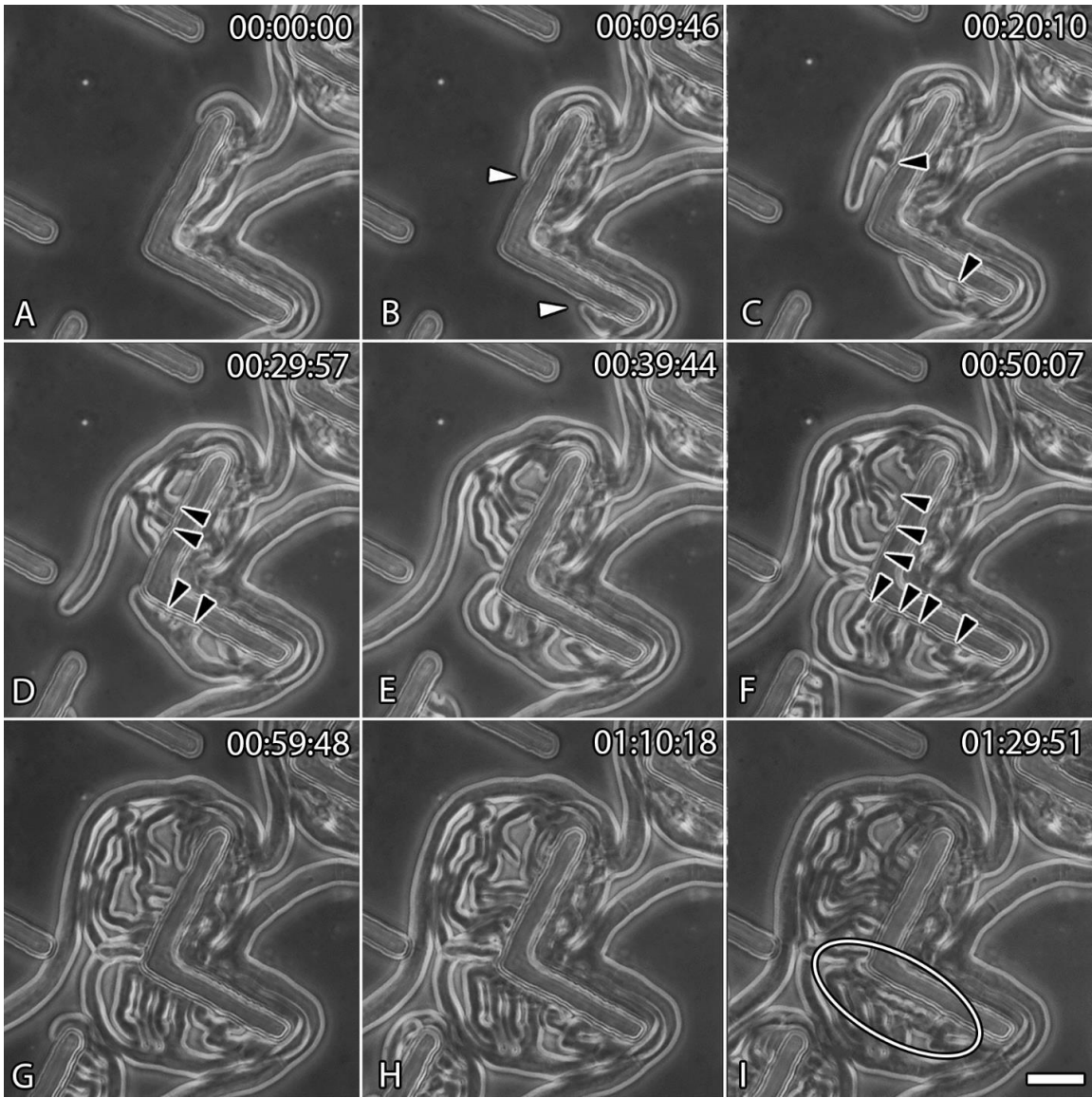
40

Figure 15. *Neurospora crassa* generating secondary and tertiary branches during two hyperbranching events. (A-B) Two hyphae of *N. crassa* round the ends of the chevron obstacle and travel along the top edge, with the white arrowheads indicating the two hyphae. (C-F) Secondary and tertiary branches begin to emerge against the chevron obstacles with the black arrowheads indicating new branches. (G-I) The new branches continue to extend and begin to overlap one another losing distinction. (I) The oval indicates the area of overlapping hyphae. Time stamp = hrs:mins:secs. Scale bar = 40µm.
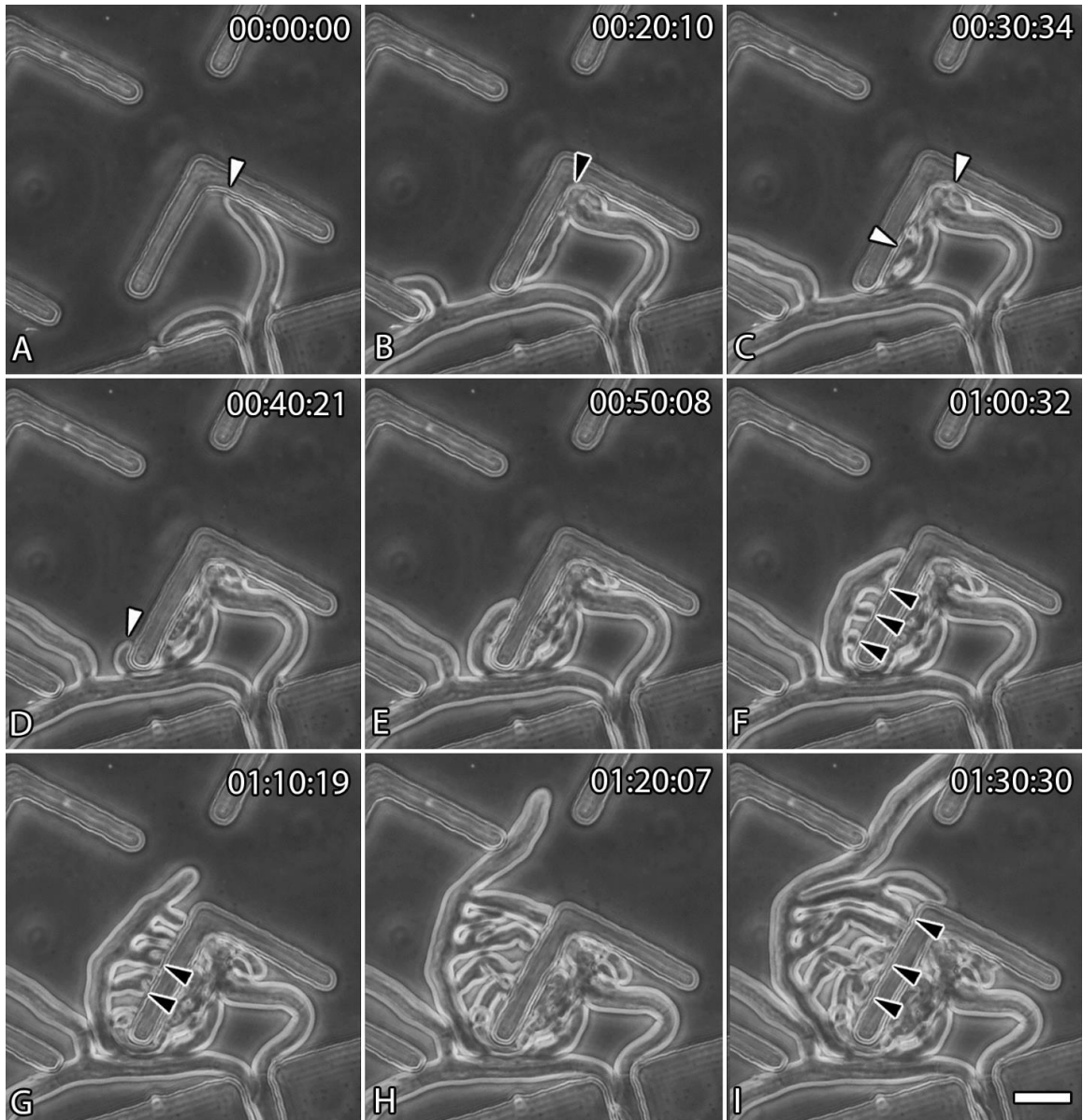
Figure 16. *Neurospora crassa* hyperbranching against the left edge of a chevron. (A) A hypha of *N. crassa* impacts near the crux of the chevron, with the white arrowhead indicating the point of impact. (B-C) The hypha travels the inner edge of the chevron and begins to branch at multiple points, with the black arrowheads indicating areas of branching. (D) A hypha escapes and rounds the edge of the chevron, with the white arrowhead indicating the hypha. (F-I) The escaped hypha begins to form secondary and tertiary branches that extend into the chevron obstacle, pushing the primary hypha away. The black arrowheads indicate the secondary and tertiary branches. Time stamp = hrs:mins:secs. Scale bar = 40µm.
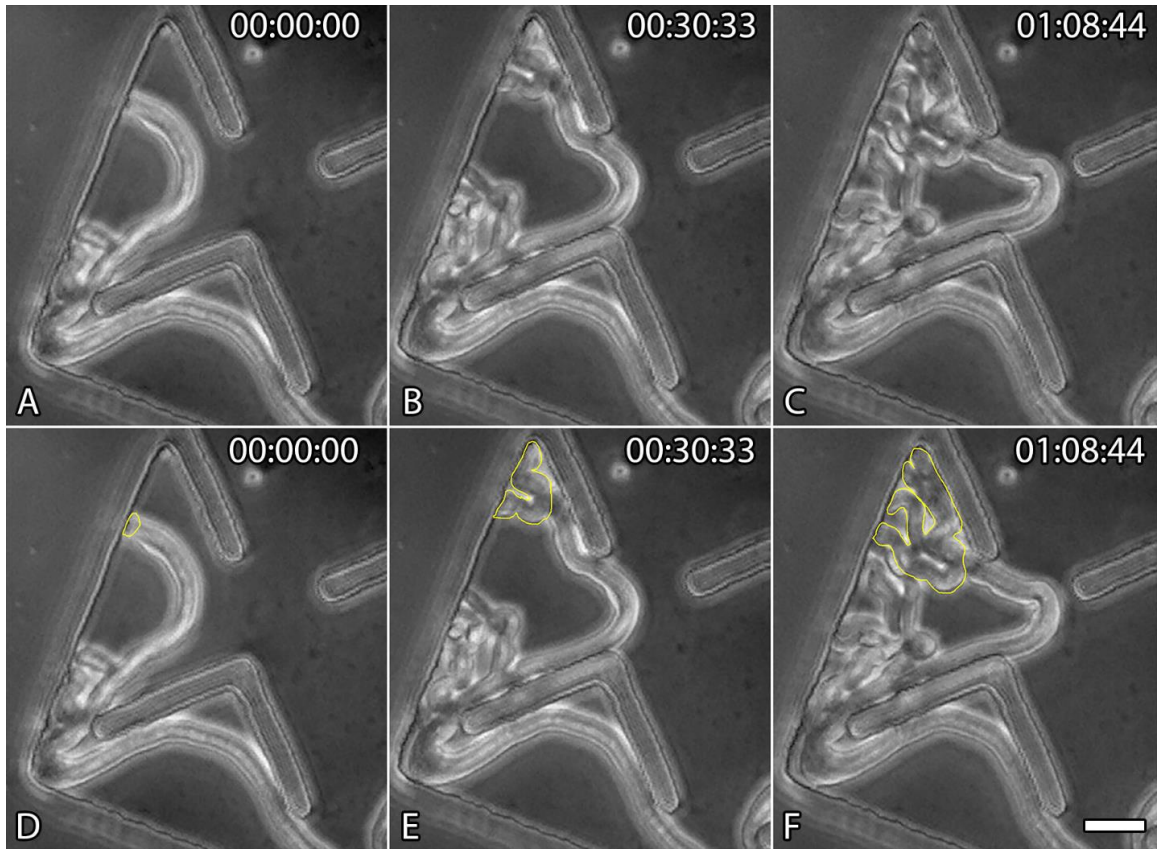
Figure 17. An example of tracing the hyperbranching event's change in area. (A-C) The hyperbranching area was measured at zero, thirty, and sixty minutes. (D-F) The yellow outline represents the manual traces. Time stamp = hrs:mins:secs. Scale bar = 20μm.

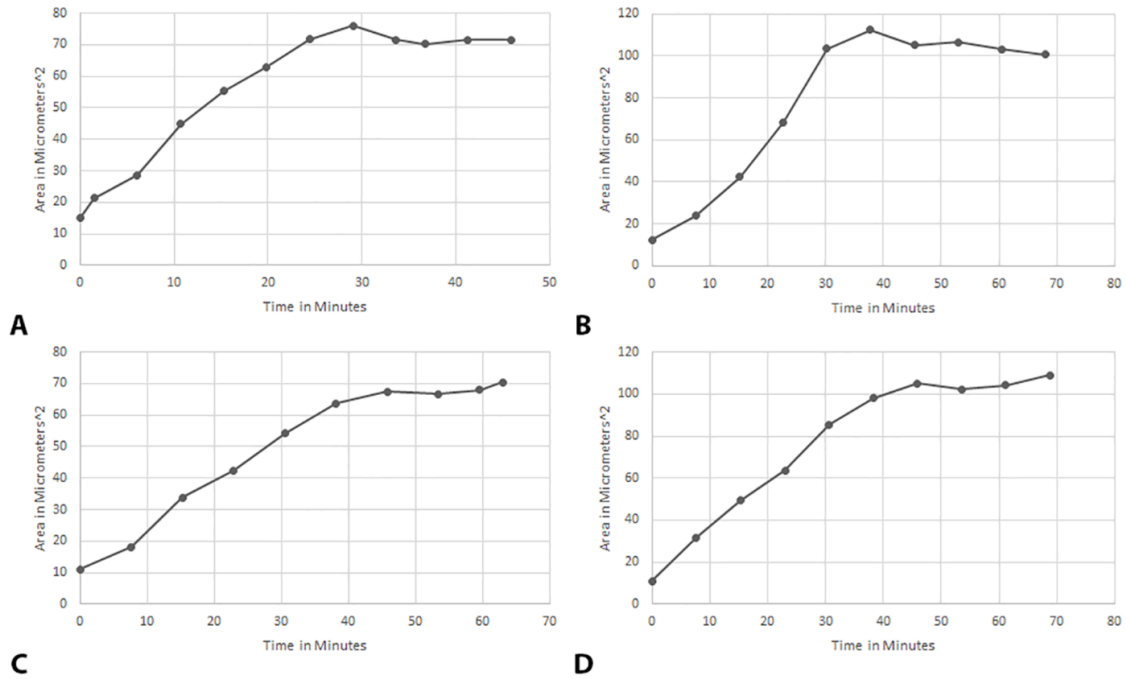**Neurospora crassa Hyperbranching Area Coverage**

Figure 18. Graphs representing the change in area during hyperbranching events. (A-D) Four hyperbranching events are represented with each chart depicting the area covered in square micrometers as it changes over time in minutes. Each hyperbranching events has an initial period of rapid expansion, before leveling off near the half hour mark.
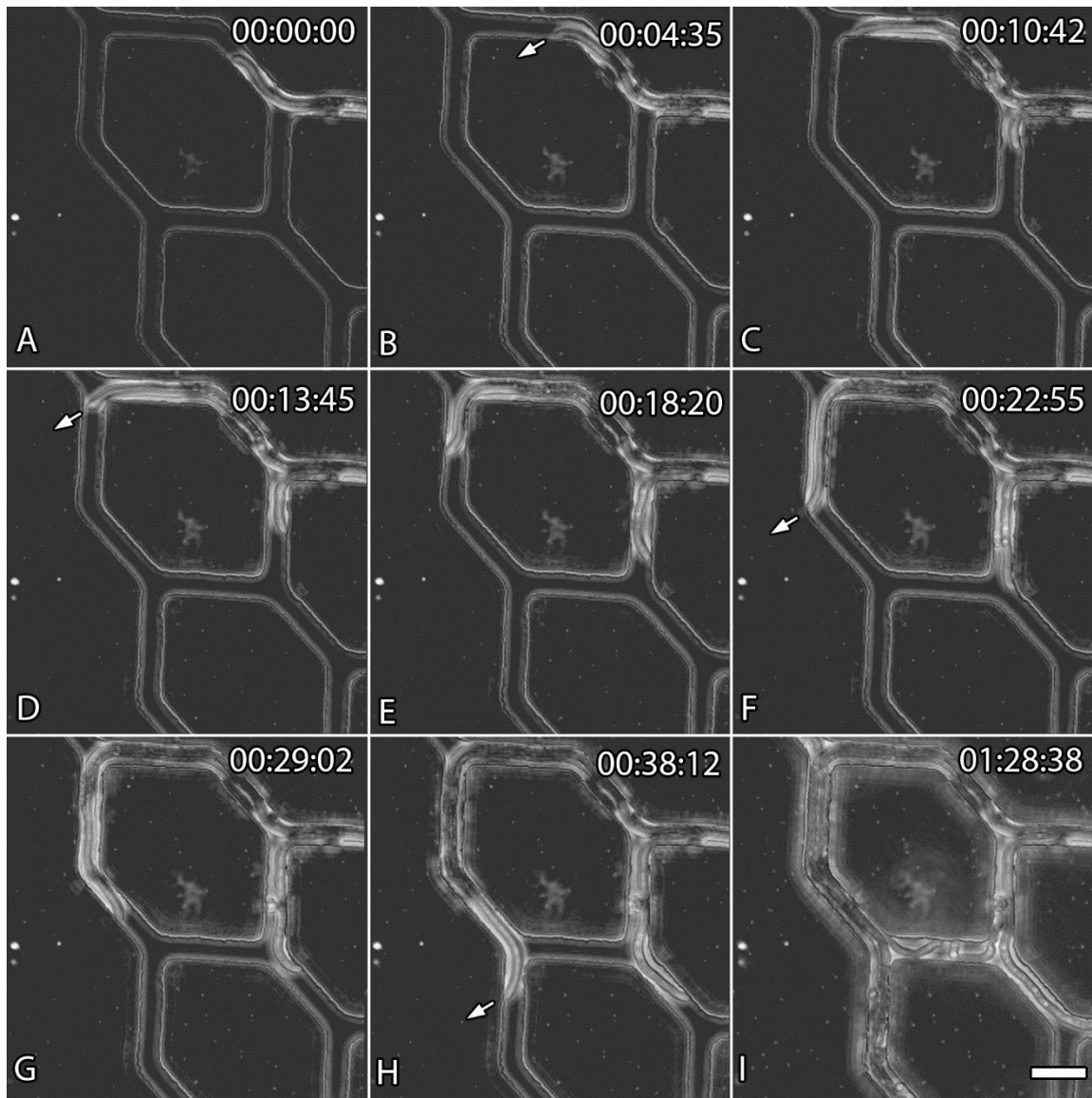
Figure 19. Directional memory of *N. crassa*. (A-C) *Neurospora crassa* can be seen arched against the diamond obstacle and retaining this arch as it rounds the top. (D-F) *Neurospora crassa* then descends the diamond obstacle but maintains its arch and its original growth direction exemplifying its directional memory. The white arrows indicate the orientation of the hyphal tip. Time stamp = hrs:mins:secs. Scale bar = 20 µm.